Supplementary Information for

Holocene paleoceanographic variability in Robertson Bay, Ross Sea, Antarctica: A marine record of ocean, ice sheet, and climate connectivity

Olivia J. Truax*, Christina R. Riesselman, Gary S. Wilson, Craig L. Stevens, Rebecca L. Parker, Jae Il Lee, Robert M. McKay, Brad Rosenheim, Catherine E. Ginnane, Jocelyn C. Turnbull, Heung Soo Moon, Min Kyung Lee, Bob Dagg, and Kyu-Cheul Yoo

***Correspondence: olivia.truax@canterbrury.ac.nz**

S1. Radiocarbon dating and RPO blank correction

All radiocarbon measurements must be corrected for any modern and dead carbon contamination that is introduced into the sample during processing. This correction is determined using measured blank materials that follow the same process as authentic samples (Donahue et al., 1990). We follow published methodologies for RPO blank correction (Table S1) (Fernandez et al., 2014; Santos et al., 2007). All graphitization and AMS radiocarbon measurements were done at the Rafter Radiocarbon Laboratory (RRL) facility, but the pre-treatment and the RPO processes were done at either University of South Florida (USF) and RRL labs, requiring slightly different blank correction procedures. For RPO, we separate blank corrections into the RPO blank and the graphitisation-measurement blank. The graphitisation-measurement modern carbon contribution is determined in the same way for all samples, and is determined from measurement of ^{14}C-free CO_2 gas from the Kapuni natural gas field (Turnbull et al., 2015), and ^{14}C-free kauri wood prepared by sealed tube combustion. The graphitisation-measurement dead carbon contribution was determined from Oxalic Acid I (Stuiver and Polach, 1977) prepared by sealed tube combustion.

USF RPO blank correction

The RPO component of the blank correction at USF is determined from geological graphite (devoid of radiocarbon, diagnosing the modern carbon contribution) and Oxalic Acid I (Ox-1, nearly modern levels of radiocarbon, diagnosing the dead carbon contribution, Stuiver and Polach, 1977) materials. To ensure the blank contamination determination is accurate for our samples, which were processed during a three-month period in 2015, we calculate blank contamination from materials processed in 2014 and 2015. We consider only “small” targets in the size range of our authentic samples, and also exclude a lot number of geological graphite that produced a low-temperature aliquot of CO_2 containing radiocarbon (Figure S1). The RPO blanks are added to the graphitization-measurement blanks. The effect of overall blank correction on reported ^{14}C values is minimal (Figure S2).

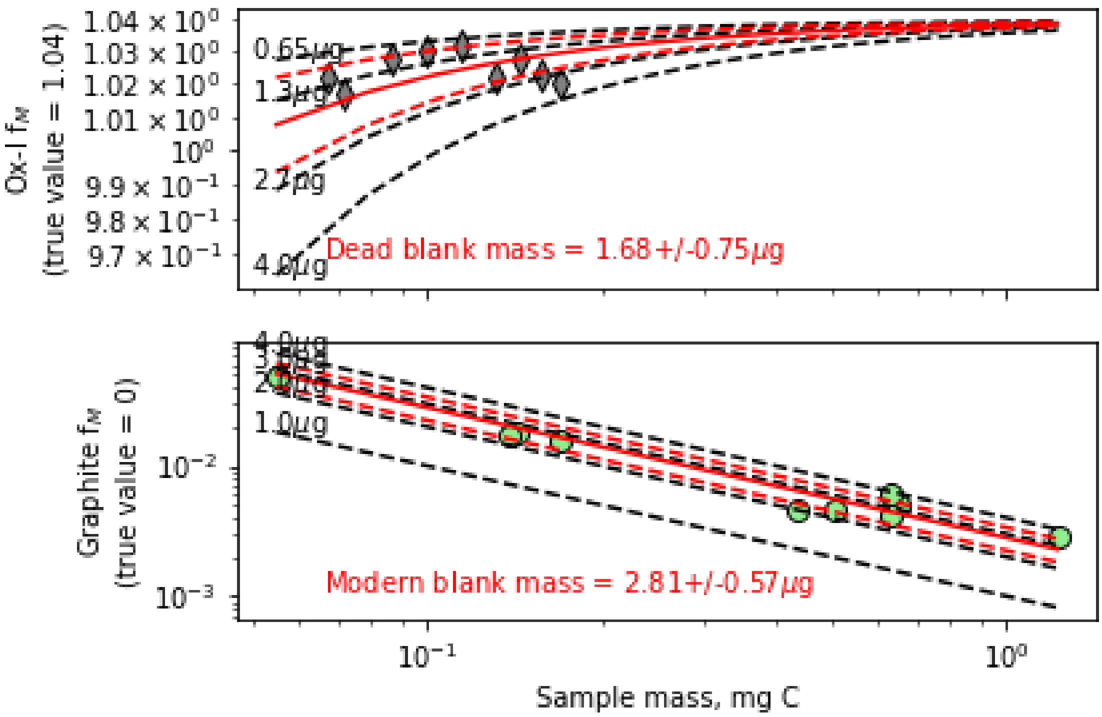

Figure S1: Samples from the USF compilation used to calculate the of blank contamination. Gray diamonds (top) show analyses of oxalic acid in the RPO system, with smaller masses deviating from the true value due to the incorporation of older (less ^{14}C) contamination. The green circles (bottom) show measurements of the radiocarbon-free graphite, which also deviate from the true value of 0 with smaller mass due to incorporation of a contaminant with radiocarbon content. The proximity of each of these data sets to lines of equal contaminant mass (dashed black lines) determines the average blank contribution and variability of the blank contribution (red solid and dashed lines, respectively).

RRL RPO blank corrections

RPO was established at RRL in 2019 in collaboration with the USF lab (Ginnane et al., 2024). The same methodology is followed as for USF-processed samples, but using radiocarbon-free kauri wood and Ox-1 as the diagnosing standard materials. Unlike USF, RRL observes a time-dependency in the modern and dead carbon blank contamination as part of the RPO process in addition to the time-independent blanks, and the correction follow standard RRL procedure for RPO samples (Ginnane et al., 2024). We note that these samples were prepared during a period when dry ice was used in the laboratory for sample processing. Dry ice is prepared from geological CO_2 and therefore can contribute dead carbon contamination through leaks of room air into the vacuum systems. More recently, dry ice has been removed from the laboratory and dead carbon contamination is substantially lower (Ginnane et al., 2024).

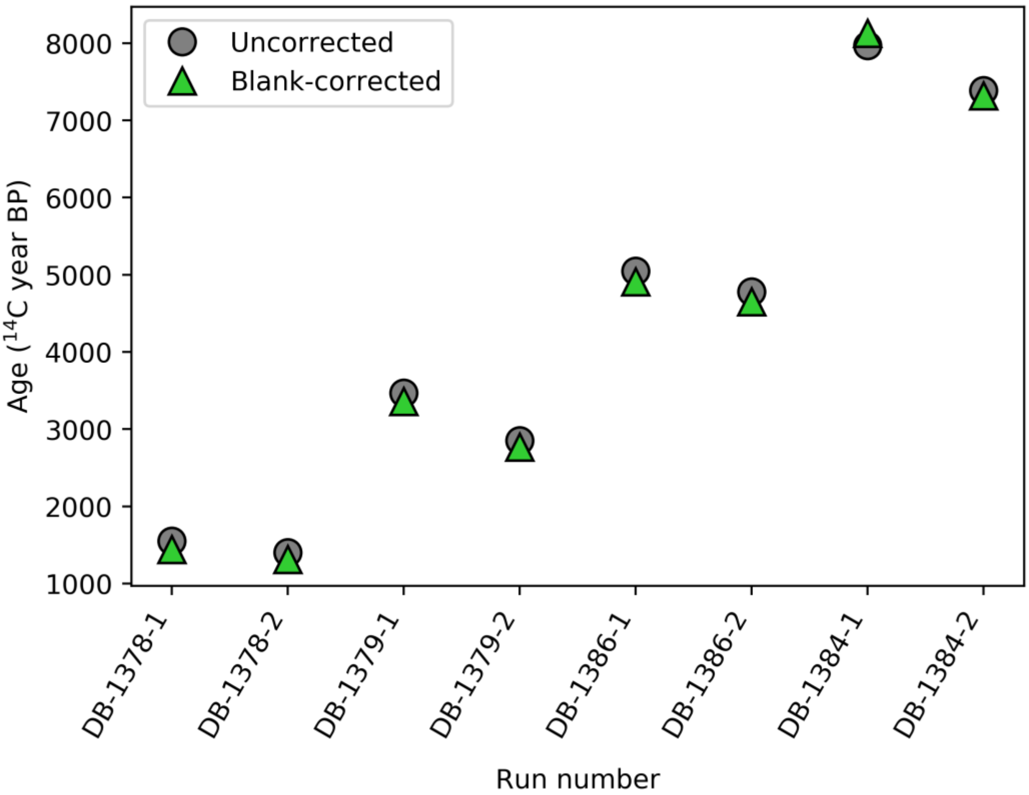

Figure S2: The effect of blank correction on reported ^{14}C values (gray circles) is minimal considering that the blank-corrected values (green triangles) are often in intersection with the uncorrected values. Smaller samples (mass not depicted in this plot) and older samples are more sensitive to blank correction.

Table S1: Reported RPO radiocarbon data from USF and RRL (denoted with an *). All dates reported in the main manuscript are calculated from the fully blank-corrected ages herein, which are corrected for graphitization and AMS at RRL and the RPO sample preparation process at USF, and then calibrated using the Marine20 calibration curve (Heaton et al., 2020) .

Sample	USF lab Identifier	RRL lab identifier	Mass (µmol)	Graphite and AMS blank corrected Fm	Graphite and AMS blank corrected uncertainty	Fully blank-corrected Fm	Fully blank-corrected uncertainty
GC57 0	DB-1378-1	NZA 62683	12.8	0.8309	0.00706	0.8363	0.00841
GC57 0	DB-1378-2	NZA 62684	15.6	0.8448	0.00563	0.8495	0.00675
GC57 180	DB-1379-1	NZA 62685	12.7	0.65818	0.00675	0.6584	0.00784
GC57 180	DB-1379-2	NZA 62686	16.0	0.70736	0.00502	0.7087	0.00594
GC57 380*	-	NZA72390	23.3	0.6029	0.00167	0.6069	0.0067
GC57 455	DB-1386-1	NZA 62696	11.5	0.54636	0.00730	0.5429	0.00841
GC57 455	DB-1386-2	NZA 62697	14.2	0.56292	0.00663	0.5606	0.00745
GC57 505*	-	NZA72389	32.4	0.4804	0.0013	0.4804	0.0027
GC57 560	DB-1384-1	NZA 62691	13.5	0.3862	0.0070	0.3787	0.00780
GC57 560	DB-1384-2	NZA 62692	16.2	0.40798	0.00445	0.4023	0.00519

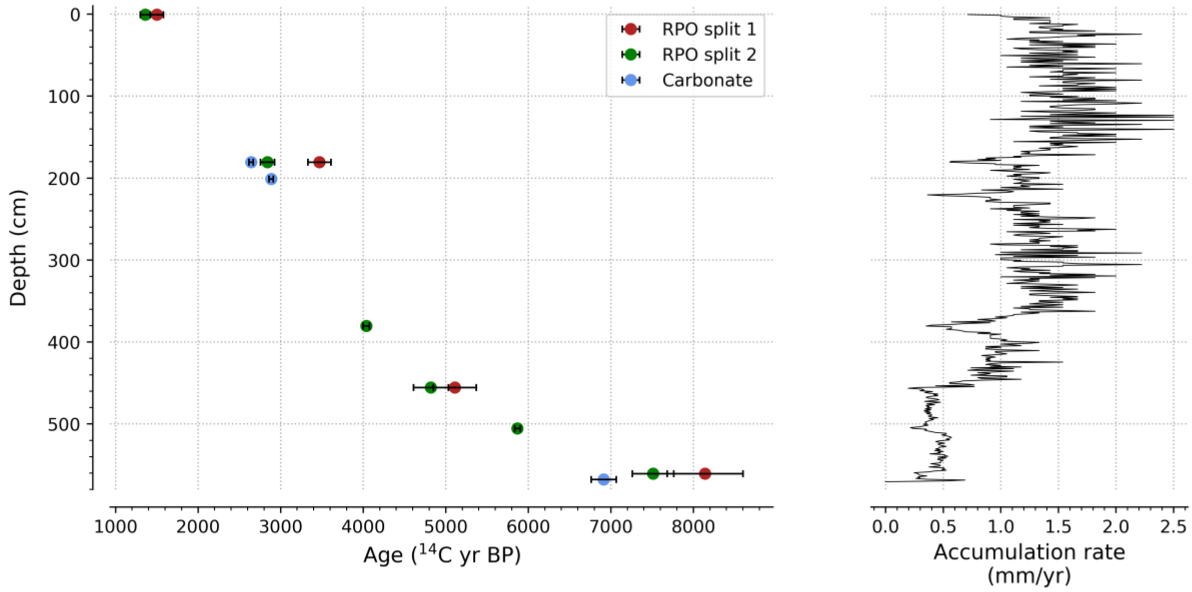

Figure S3: radiocarbon ages and accumulation rate for core RS15-GC57; uncalibrated radiocarbon ages (^{14}C yr BP) and uncertainties (left) and accumulation rate (mm/yr) derived from the calibrated age model (right).

S2. Modern instrumental data

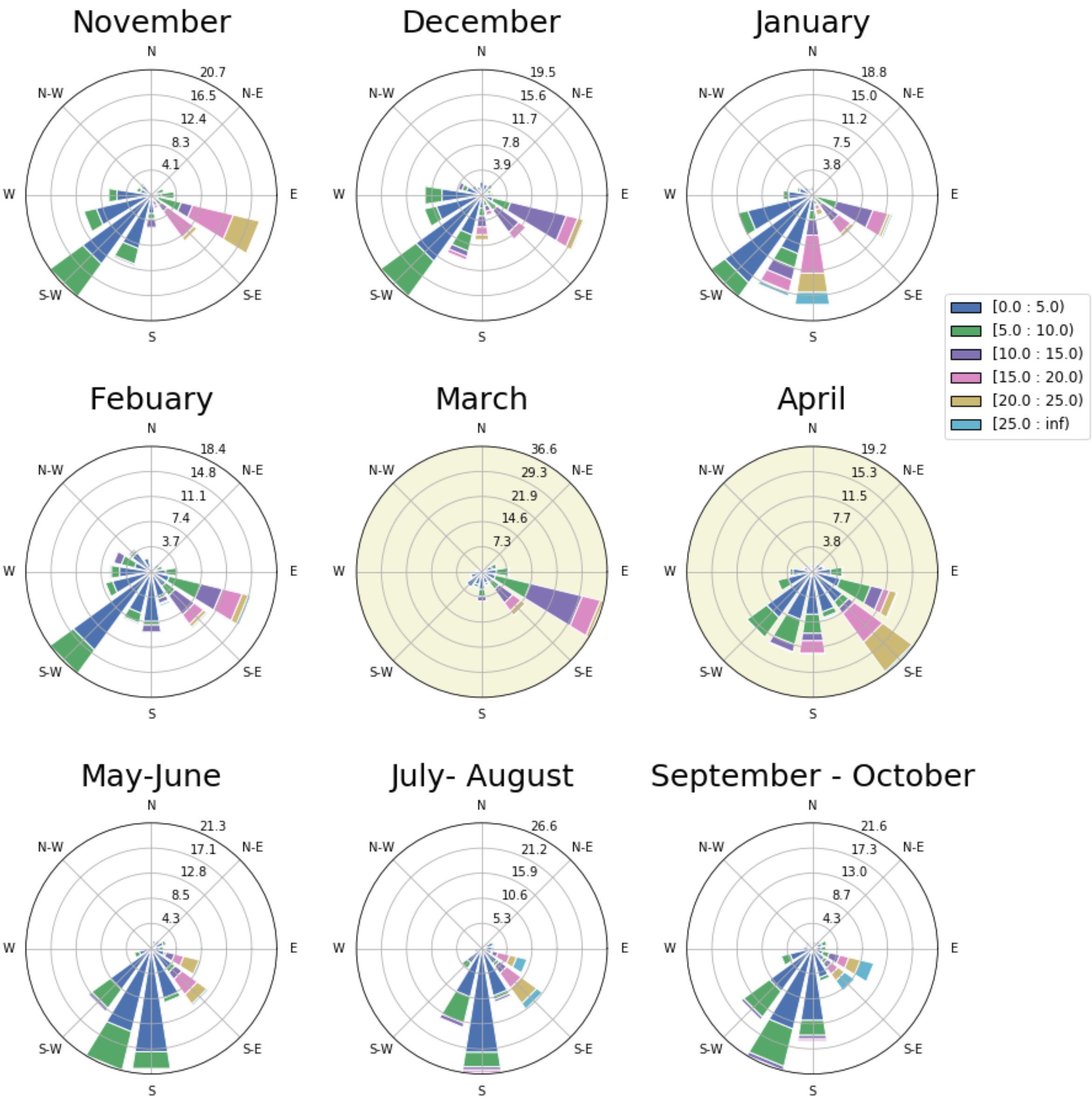

Figure S4: Proportion of prevailing winds by direction strength (meters per second) along the Cape Adare Ridge in between November 2015 and November 2016. An increase in the wind speed (color) and shift to the southeast occurs during sea ice advance in March and April and is highlighted in beige.

S3. Supplementary information about proxy records

Table S2: Correlation (R value) of paleoclimate records. Proxies associated with primary productivity (Br/Ti, TOC, wt% BSi, ADA) are corelated with each other (R>0, highlighted in red) and anti-corelated (R<0, highlighted in blue) with MS, a proxy for terrigenous sediment. D13C and sand percentage are positively corelated with MS.

	MS	$\delta^{13}C$	Sand abundance	Br/Ti	TOC	Wt% BSi	TN	ADA
MS	1	0.84	0.76	-0.57	-0.71	-0.82	-0.76	-0.42
$\delta^{13}C$	0.84	1	0.75	-0.53	-0.68	-0.83	-0.68	-0.38
Sand	0.76	0.75	1	-0.58	-0.69	-0.75	-0.75	-0.4
Br/Ti	-0.57	-0.53	-0.58	1	0.71	0.57	0.71	0.54
TOC	-0.71	-0.68	-0.69	0.71	1	0.7	0.87	0.58
Wt% BSi	-0.82	-0.83	-0.75	0.57	0.7	1	0.72	0.5
TN	-0.76	-0.68	-0.75	0.71	0.87	0.72	1	0.51
ADA	-0.42	-0.38	-0.4	0.54	0.58	0.5	0.51	1

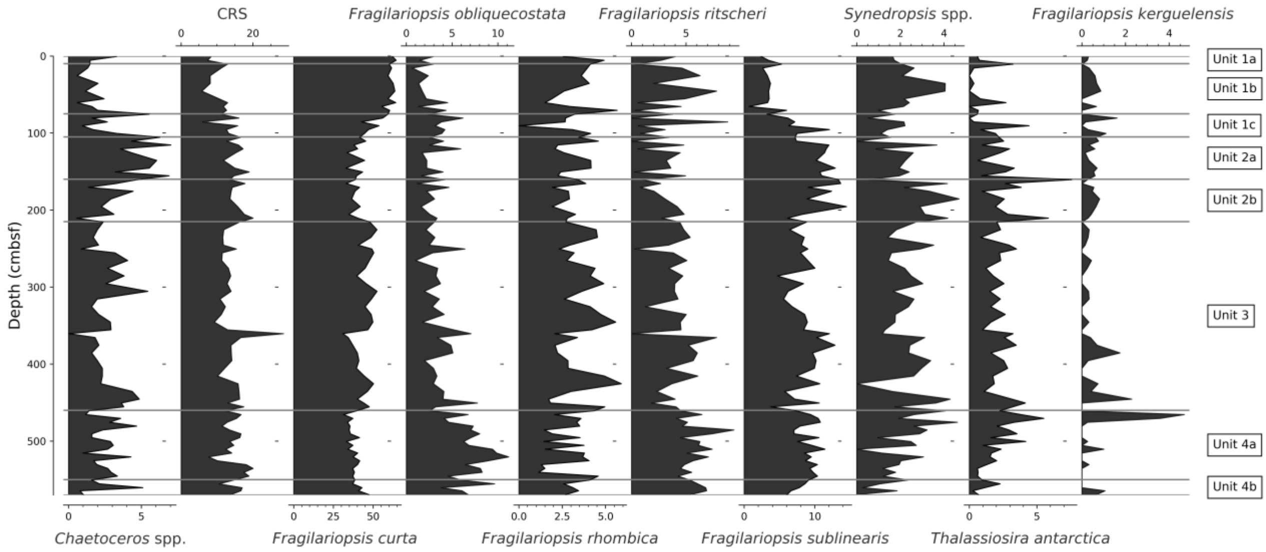

Figure S5: Relative abundance of diatoms taxa with relative abundance greater than 5% in core RS15-GC57.

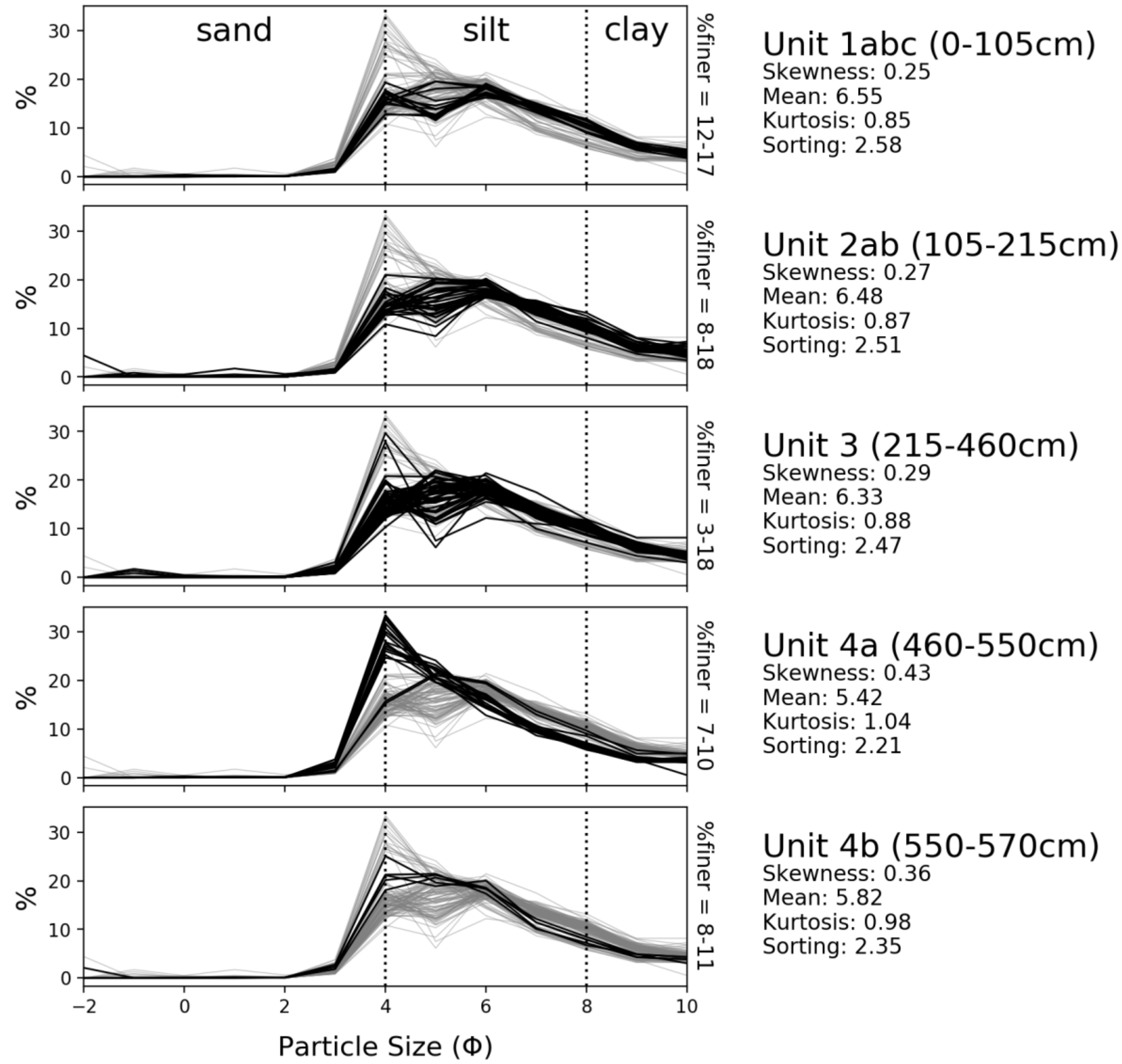

Figure S6: Grainsize analysis for each sedimentary unit and average skewness, sorting, kurtosis, and grainsize. Full core shown in grey and each is unit highlighted in black. Units 1, 2, and 3 are dominated by silt. Unit 4a is distinguished by an increase in the proportion of coarse silt and very find sand and a more well sorted, coarse skewed grainsize assemblage.

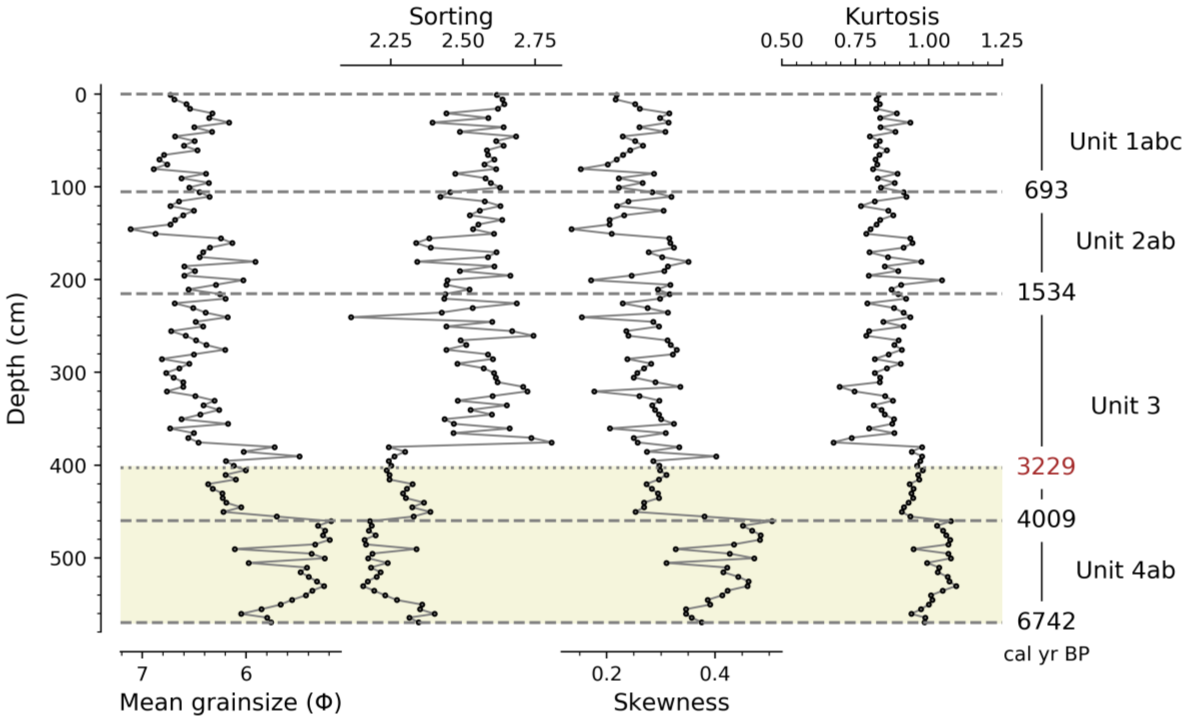

Figure S7: Down-core profiles of grainsize summary statistics (mean grainsize, sorting, skewness, and kurtosis) for core GC57. Sedimentary units highlighted by dashed lines; dotted line indicates the transition from laminated sandy muds (570-403 cm, beige) to pervasively bioturbated biosilica-bearing muds (403-0 cm).

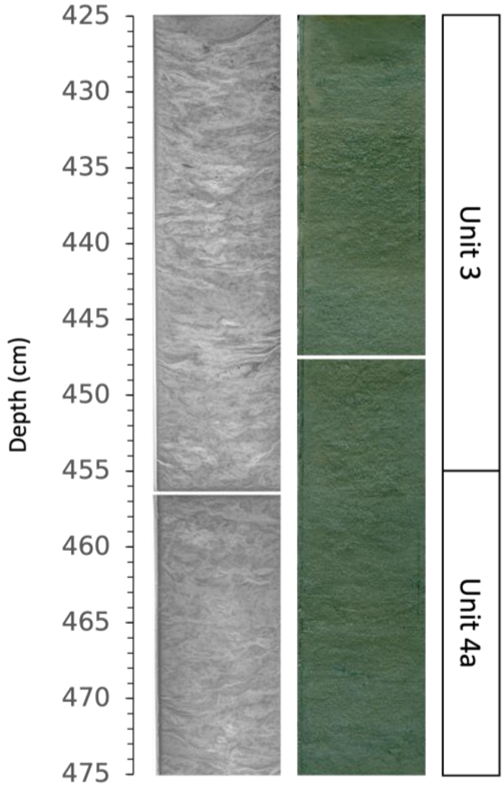

Figure S8: Core slab X-ray with ripple filter (left) and core photograph (right) showing no evidence of a hiatus at the boundary between Unit 4 and Unit 3.

S4. Method for aligning data from CTD cast and hydrographic moorings

We correct measurements of salinity, potential temperature, and dissolved oxygen from the Sea-Bird SBE 19 CTD cast using contemporaneous measurements from Sea-Bird SBE 37-SMP-ODO CTDs deployed on shallow (45 and 53 m) and deep (302) hydrographic moorings. Mean offsets of 3.62 mg/L (dissolved oxygen), 0.18 psu (salinity), and 0.4˚C (potential temperature) between the CTD cast and the hydrographic moorings are within the uncertainty of Sea-Bird field deployments. Excellent agreement between the shallow moorings at 45 and 53 m depth, which were factory calibrated, provides confidence in CTD measurements from the moorings.

Table S1: comparison between salinity, potential temperature, and dissolved oxygen measurements from the CTD cast taken on Nov. 7th 2015 and mean values for moorings deployed at the same depth between Nov 2nd and Nov 12th 2015.

	45 m depth			53 m depth			302 m depth			Mean offset
	CTD cast	Mooring	Offset	CTD cast	Mooring	Offset	CTD cast	Mooring	Offset	
Potential temperature (˚C)	-1.76	-1.81	-0.05	-1.76	-1.82	-0.05	-1.74	-1.74	0.00	-0.03
Dissolved oxygen (mg/L)	5.12	8.68	3.57	5.02	8.39	3.37	4.90	8.82	3.91	3.62
Salinity (psu)	34.15	34.00	-0.15	34.20	34.01	-0.19	34.43	34.25	-0.18	-0.17

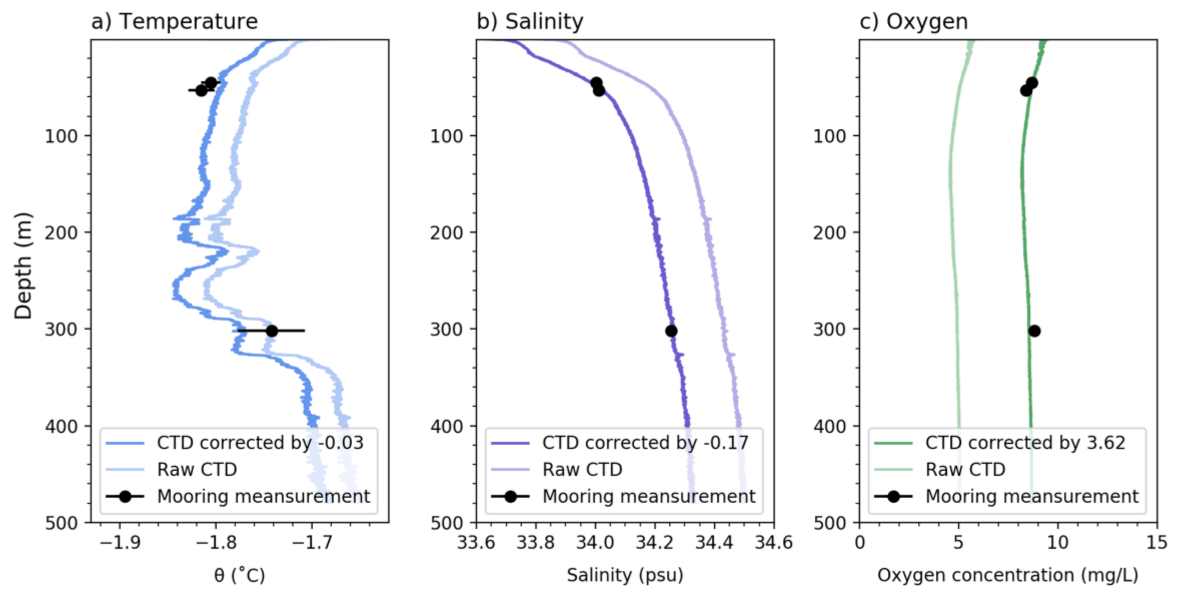

Figure S9: Offset between raw measurements from the Sea-Bird SBE 19 CTD cast and profiles corrected using mean measurements from Sea-Bird SBE 37-SMP-ODO CTDs deployed on shallow (45 and 53 m) and deep (302) hydrographic moorings. Black dots show average mooring measurements 5 days before and after the CTD cast, error bars highlight the standard deviation for the 11-day period.

References:

Donahue, D.J., Linick, T.W., Jull, A.J.T., 1990. Isotope-Ratio and Background Corrections for Accelerator Mass Spectrometry Radiocarbon Measurements. Radiocarbon 32, 135–142. https://doi.org/10.1017/S0033822200040121

Fernandez, A., Santos, G.M., Williams, E.K., Pendergraft, M.A., Vetter, L., Rosenheim, B.E., 2014. Blank Corrections for Ramped Pyrolysis Radiocarbon Dating of Sedimentary and Soil Organic Carbon. Anal. Chem. 86, 12085–12092. https://doi.org/10.1021/ac502874j

Ginnane, C.E., Turnbull, J.C., Naeher, S., Rosenheim, B.E., Venturelli, R.A., Phillips, A.M., Reeve, S., Parry-Thompson, J., Zondervan, A., Levy, R.H., Yoo, K.-C., Dunbar, G., Calkin, T., Escutia, C., Pastor, J.G., 2024. Advancing antarctic sediment chronology through combined Ramped Pyrolysis Oxidation and Pyrolysis-GC-MS. Radiocarbon 1–20. https://doi.org/10.1017/RDC.2023.116

Heaton, T.J., Köhler, P., Butzin, M., Bard, E., Reimer, R.W., Austin, W.E.N., Ramsey, C.B., Grootes, P.M., Hughen, K.A., Kromer, B., Reimer, P.J., Adkins, J., Burke, A., Cook, M.S., Olsen, J., Skinner, L.C., 2020. Marine20—The Marine Radiocarbon Age Calibration Curve (0–55,000 cal BP). Radiocarbon 62, 779–820. https://doi.org/10.1017/RDC.2020.68

Santos, G.M., Moore, R.B., Southon, J.R., Griffin, S., Hinger, E., Zhang, D., 2007. AMS ^{14}C Sample Preparation at the KCCAMS/UCI Facility: Status Report and Performance of Small Samples. Radiocarbon 49, 255–269. https://doi.org/10.1017/S0033822200042181

Stuiver, M., Polach, H.A., 1977. Discussion Reporting of ^{14}C Data. Radiocarbon 19, 355–363. https://doi.org/10.1017/S0033822200003672